Title

AAV8-Mediated In Vivo Overexpression of miR-155 Enhances the Protective Capacity of Genetically Attenuated Malarial Parasites

Journal

Molecular Therapy, 22(12)

ISSN

1525-0016

Authors

Hentzschel, Franziska
Hammerschmidt-Kamper, Christiane
Börner, Kathleen
et al.

Publication Date

2014-12-01

DOI

10.1038/mt.2014.172

Peer reviewed

AAV8-Mediated *In Vivo* Overexpression of miR-155 Enhances the Protective Capacity of Genetically Attenuated Malarial Parasites

Franziska Hentzschel[1,2], Christiane Hammerschmidt-Kamper[1], Kathleen Börner[2], Kirsten Heiss[1], Bettina Knapp[3,4,5,6], Julia M Sattler[1], Lars Kaderali[3,4,5], Mirco Castoldi[7], Julia G Bindman[8], Yann Malato[9], Holger Willenbring[8,9,10], Ann-Kristin Mueller[1] and Dirk Grimm[2,4]

[1]Centre for Infectious Diseases, Parasitology, Heidelberg University Hospital, Heidelberg, Germany; [2]Centre for Infectious Diseases, Virology, Heidelberg University Hospital, Heidelberg, Germany; [3]ViroQuant Research Group Modeling, BioQuant, University of Heidelberg, Heidelberg, Germany; [4]Cluster of Excellence CellNetworks, Heidelberg, Germany; [5]Medical Faculty Carl Gustav Carus, Institute for Medical Informatics and Biometry, Dresden University of Technology, Dresden, Germany; [6]Institute of Computational Biology, Helmholtz Zentrum München – German Research Center for Environmental Health, Neuherberg, Germany; [7]University Hospital Düsseldorf, Gastroenterology, Hepatology and Infectious Diseases, Düsseldorf, Germany; [8]Department of Surgery, Division of Transplantation, University of California San Francisco, San Francisco, California, USA; [9]Eli and Edythe Broad Center of Regeneration Medicine and Stem Cell Research, University of California San Francisco, San Francisco, California, USA; [10]Liver Center, University of California San Francisco, San Francisco, California, USA.

Malaria, caused by protozoan *Plasmodium* parasites, remains a prevalent infectious human disease due to the lack of an efficient and safe vaccine. This is directly related to the persisting gaps in our understanding of the parasite's interactions with the infected host, especially during the clinically silent yet essential liver stage of *Plasmodium* development. Previously, we and others showed that genetically attenuated parasites (GAP) that arrest in the liver induce sterile immunity, but only upon multiple administrations. Here, we comprehensively studied hepatic gene and miRNA expression in GAP-injected mice, and found both a broad activation of IFNγ-associated pathways and a significant increase of murine microRNA-155 (miR-155), that was especially pronounced in non-parenchymal cells including liver-resident macrophages (Kupffer cells). Remarkably, ectopic upregulation of this miRNA in the liver of mice using robust hepatotropic adeno-associated virus 8 (AAV8) vectors enhanced GAP's protective capacity substantially. In turn, this AAV8-mediated miR-155 expression permitted a reduction of GAP injections needed to achieve complete protection against infectious parasite challenge from previously three to only one. Our study highlights a crucial role of mammalian miRNAs in *Plasmodium* liver infection *in vivo* and concurrently implies their great potential as future immune-augmenting agents in improved vaccination regimes against malaria and other diseases.

Received 5 December 2013; accepted 25 August 2014; advance online publication 7 October 2014. doi:10.1038/mt.2014.172

INTRODUCTION

More than 130 years after the discovery of the underlying infectious agent, the single-celled *Plasmodium* parasite is still responsible for 250 million clinical cases and around 1 million deaths per year (http://www.who.int/topics/malaria/en/). Moreover, it is currently estimated that 40% of the world's population remain at risk for malaria infection.[1,2] A major reason for the persistence of this disease in humans is the lack of a potent vaccine, a direct consequence of the persisting gaps in our understanding of the *Plasmodium* interactions with its infected host *in vivo*. The latter especially pertains to the clinically silent liver stage, which remains even more enigmatic than the pathogenic erythrocytic stages. In liver cells, the differentiating and replicating parasite resides in a membranous compartment named parasitophorous vacuole, separating it from the host-cell cytoplasm in addition to its own plasma membrane.[3] To date only few vital host factors required for the successful establishment of malarial intra-hepatic development have been identified. For instance, downregulation of both liver-fatty acid binding protein (L-FABP) and the lipoprotein receptor scavenger receptor type B class I (SR-BI) impairs *Plasmodium* liver-stage development.[4,5] In addition, a very recent study highlighted the importance of innate immune mediators of the type I interferon (IFN) pathway for *Plasmodium* intra-hepatic progression.[6]

As *Plasmodium* differentiation in the host liver is a prerequisite for the onset of malaria, inhibition of hepatic parasite replication represents a potent approach for disease prevention. Indeed, radiation- or genetically attenuated parasites (RAS or GAP, respectively) that arrest within the liver can confer sterile immunity.[7,8] Thus far, repeated immunization of humans and rodents with gamma-irradiated sporozoites (the parasite form that develops

The first four authors contributed equally to this work.

Correspondence: Ann-Kristin Mueller, Centre for Infectious Diseases, Parasitology Unit, Im Neuenheimer Feld 324, 69120 Heidelberg, Germany. E-mail: ann-kristin.mueller@uni-heidelberg.de or Dirk Grimm, Centre for Infectious Diseases/Virology, BioQuant BQ0030, Im Neuenheimer Feld 267, 69120 Heidelberg, Germany. E-mail: dirk.grimm@bioquant.uni-heidelberg.de

in the salivary mosquito glands and infects the host liver after transmission) is the only experimental vaccine that yields complete protection and remains the gold standard.[7,9,10] Still, as genetic attenuation yields far more homogenous and defined parasite populations than irradiation, GAP is an attractive alternative to RAS as a whole-organism malaria vaccine in humans. However, two major concerns hamper the further development and application of GAP vaccines—the need for successive administrations, and our poor knowledge of the underlying antigen-specific effector mechanisms. Evidence to date suggests that protection induced by attenuated parasites relies on cytotoxic $CD8^+$ T cells and $CD4^+$ T helper cells, implying that in particular the cellular arm of the immune system is engaged.[11–13] Furthermore, a crucial role for the pro-inflammatory cytokine IFN-γ in the induction of sterile immunity has been repeatedly demonstrated.[11–15]

In this study, we have further dissected the potential role of genes and miRNAs as two related classes of host factors during attenuated liver infection of mice harboring *P. berghei uis3(-)* mutant parasites. These GAP parasites lack the vital liver-stage specific gene *uis3* and are believed to display arrested growth during liver-stage development around 24 hours after infection.[8] We were particularly interested in miRNAs (short for microRNAs) since these molecules are predicted to be master regulators of at least 60% of all mammalian genes and are known to play central roles in pathological processes, including cancer and pathogen infections.[16,17] We find that GAP injection induces a rapid and strong increase of miR-155, a mammalian miRNA with a central role in the control of innate and adaptive immunity. In addition, we show that GAP infusion stimulates TNFα and IFNγ expression, two known upstream regulators of miR-155, and activates associated cellular pathways. Finally, we demonstrate that ectopic upregulation of miR-155 using hepatotropic adeno-associated viral gene transfer vectors substantially improves vaccination of mice against wild-type *Plasmodium* challenge. Evidence is that pretreatment of mice with the miR-155-expressing vector reduced the amount of GAP injections needed to achieve complete immunity against the wild-type parasite from previously three to only one. Our study fundamentally enhances our knowledge on the natural interactions between *Plasmodium* and its infected host during the liver stage, and at the same time suggests that ectopic dysregulation of endogenous miRNAs and/or their cognate targets may be harnessed as a novel strategy to improve vaccination against malaria and other infectious diseases.

RESULTS

Gene and miRNA expression in *Plasmodium*-infected mouse livers

We initially aimed to extend our mechanistic understanding of *Plasmodium*-host interactions, and therefore studied the expression of hepatic genes and miRNAs in mice inoculated with attenuated as compared to wild-type (WT) parasites. Interestingly, whole liver cDNA profiling 24 or 40–44 hours after GAP inoculation showed a broad activation especially of cellular pathways associated with interferon γ- (IFNγ) and tumor necrosis factor α- (TNFα) regulated gene expression (**Figure 1a**, **Supplementary Figure S1 and Tables S1–S4**). Quantitative real-time PCR (qRT-PCR) analysis validated increased IFNγ and TNFα cDNA levels in both GAP- and WT-infected versus naïve livers that were consistently significant for GAP (**Figure 1b**). Notable downstream targets of these two factors that were overexpressed in GAP-inoculated mice included the two T-cell chemoattractants *cxcl9* (also known as Monokine induced by IFNγ, MIG) and *cxcl10* (**Supplementary Tables S1–S4**). Also elevated were *mmd2* (monocyte to macrophage differentiation-associated 2), *gbp2* (IFNγ-induced guanylate-binding protein 2) and three isoforms of acute-phase serum amyloid A proteins (*SAA1-3*), *i.e.*, TNFα-induced hepatic factors known to increase in response to inflammatory stimuli.[18]

Concurrently, we measured the expression of 698 murine miRNAs in the same samples (also including RAS in this experiment) using microarrays. Of these, 157 crossed a cutoff of 1.2 for the signal-to-noise ratio (**Supplementary Table S5**). Moreover, 29 of the 698 miRNAs were significantly dysregulated between the six experimental groups (WT, GAP, RAS; 24 or 40 hours) (**Figure 1c**). The overlap between the two categories was 11 miRNAs (highlighted with arrows in **Supplementary Table S5** and **Figure 1c**). By far most abundant among the 157 miRNAs—yet not dysregulated as compared to naïve mice—was miR-122, as expected in the liver.[19] Also notable was miR-21 as it was consistently detected and increased versus naïve mice in all cohorts (**Figure 1c**; validated by qRT-PCR in **Supplementary Figure S2a,b**). In contrast, several other known immuno-regulatory miRNAs were either unaltered (*e.g.*, miR-125b and miR-146) or not detected at all (miR-155). This seemed curious in light of the results of our pathway analyses and in view of the known role of miRNAs as immune modulators.[20] However, one likely explanation was that sporozoites only infect a minority of hepatocytes,[21] suggesting that global microarray profiling may have underestimated subtle fluctuations.

Identification of miR-155 upregulation in GAP-infected mice

This possibility tempted us to re-screen identical mouse cohorts for changes in selected immuno-regulatory miRNAs using more sensitive qRT-PCR. Next to whole livers, we additionally segregated hepatocytes from non-parenchymal cells (NPC) including liver-resident macrophages (Kupffer cells, a source of immuno-regulatory miRNAs) (see **Supplementary Figure 3** for workflow), based on evidence that the malaria parasite traverses Kupffer cells to gain full infectivity in hepatocytes.[22] This refined strategy indeed revealed a significant upregulation particularly of one immuno-regulatory miRNA, miR-155, both in total livers and in the NPC fraction (**Figure 2a**,**b**). Moreover, we measured miR-155 levels in blood exosomes but found no evidence for secretion and extracellular trafficking of this miRNA (**Supplementary Figure S2c**). The miR-155 upregulation in the liver samples was consistently observed on the level of both precursor and mature miR-155, suggesting an increase in miR-155 transcription rather than processing (**Supplementary Figure S2d**). The elevation of miR-155 in total livers was especially pronounced 24 hours after GAP inoculation (**Figure 2a**), and it was additionally confirmed using a miR-155-sensitive luciferase reporter that showed GAP-dependent inhibition in livers of infected mice (**Figure 2c–f**, orange bars; the decrease in luciferase expression reflects an increase in the miRNA in GAP-treated mice). Notably, miR-155 is known to be synergistically and rapidly induced by IFNγ and TNFα,[23,24] well

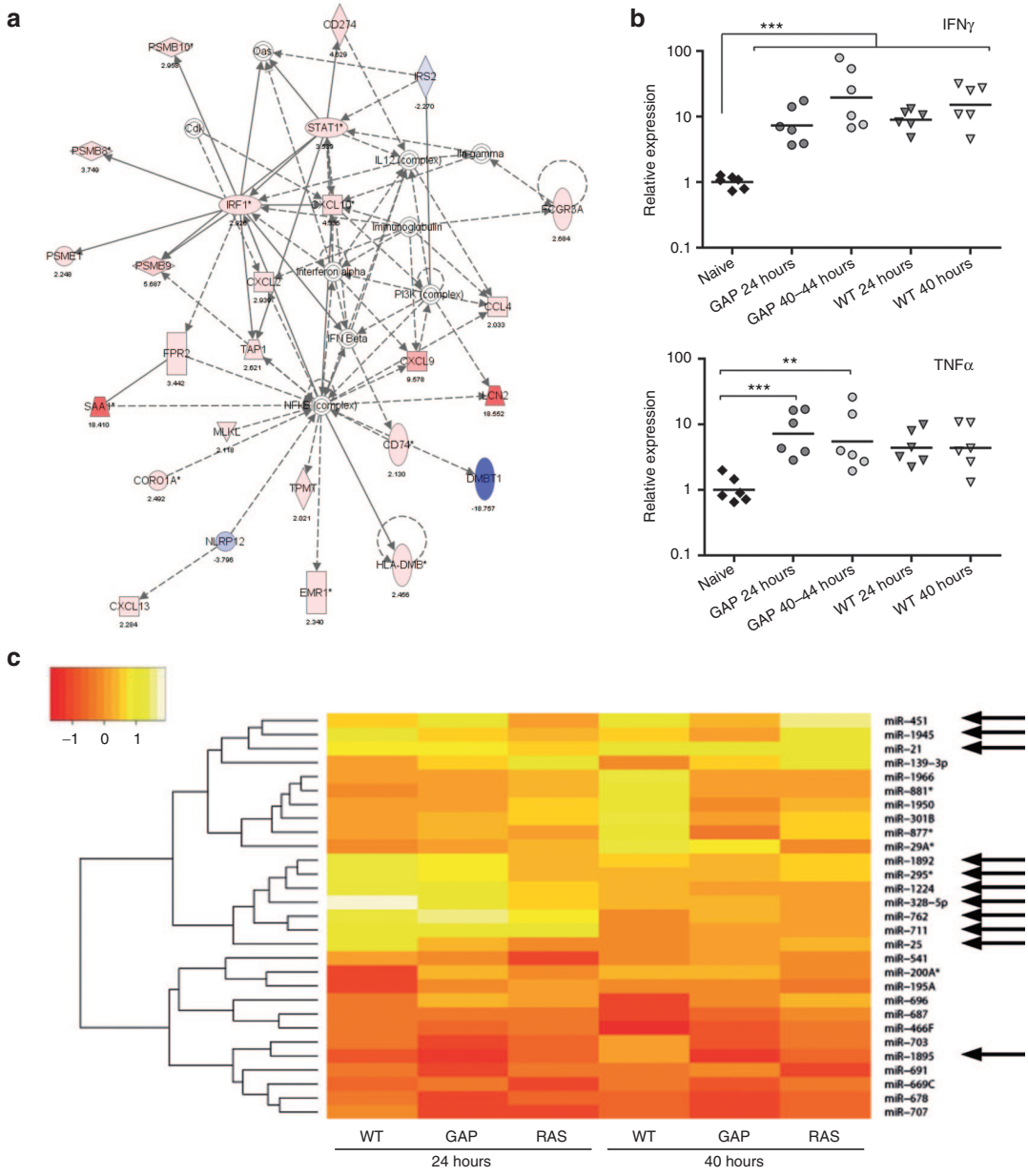

Figure 1 Analysis of gene and miRNA expression in livers of *Plasmodium*-infected mice. (**a**) Representative pathways (drawn using Ingenuity software) mapping to immunological disease that are altered 40–44 hours after GAP infection (red: upregulated genes, blue: downregulated genes). (**b**) qRT-PCR–based validation of IFNγ and TNFα upregulation in the indicated mouse cohorts. $^{**}P < 0.01$, $^{***}P < 0.001$ (one-way analysis of variance, Dunnett's test). (**c**) Heatmap depicting the median of the fold-change values of the 29 miRNAs which have been significantly differentially expressed in comparison to naïve mice in at least one of the experimental settings (WT, GAP or RAS at 24 or 40 hours) of the microarray analysis. Highlighted with arrows are the 11 miRNAs which also had a SNR >1.2 (see also **Supplementary Table S5**).

in line with our notion of an upregulation of these two genes in the same liver samples (**Figure 1b** above). Indeed, we also noted a pronounced and statistically significant 4.5- to 12.7-fold (IFNγ) and 2.0- to 4.5-fold (TNFα) increase of these two factors in the NPC fraction especially in the GAP-treated mice (**Figure 3a**,**b**). We moreover found a concomitant *Plasmodium*-induced increase of two of the best characterized miR-155 targets with an immunoregulatory function, SOCS1 and SHIP1,[25,26] in the hepatocyte as well as the NPC fraction (**Figure 3c**,**d**). A likely interpretation of all these data is that *Plasmodium*, especially attenuated GAP parasites, provokes a rapid and strong pro-inflammatory host response consisting of an induction of IFNγ/TNFα signaling. This in turn results in a spike of miR-155 particularly in the NPC fraction containing liver-resident macrophages. The notion that SOCS1 and SHIP1 are elevated despite the miR-155 increase initially appears counter-intuitive but is in fact well in line with their biology. This is because, akin to miR-155, they are also induced by cytokines including IFNγ and can then act in a negative feedback loop to attenuate the immune response (see also Discussion).

miR-155 is particularly upregulated in the Kupffer cell fraction in GAP-infected livers

The NPC fraction obtained with the workflow used above (**Supplementary Figure S3**) represented a mixture of

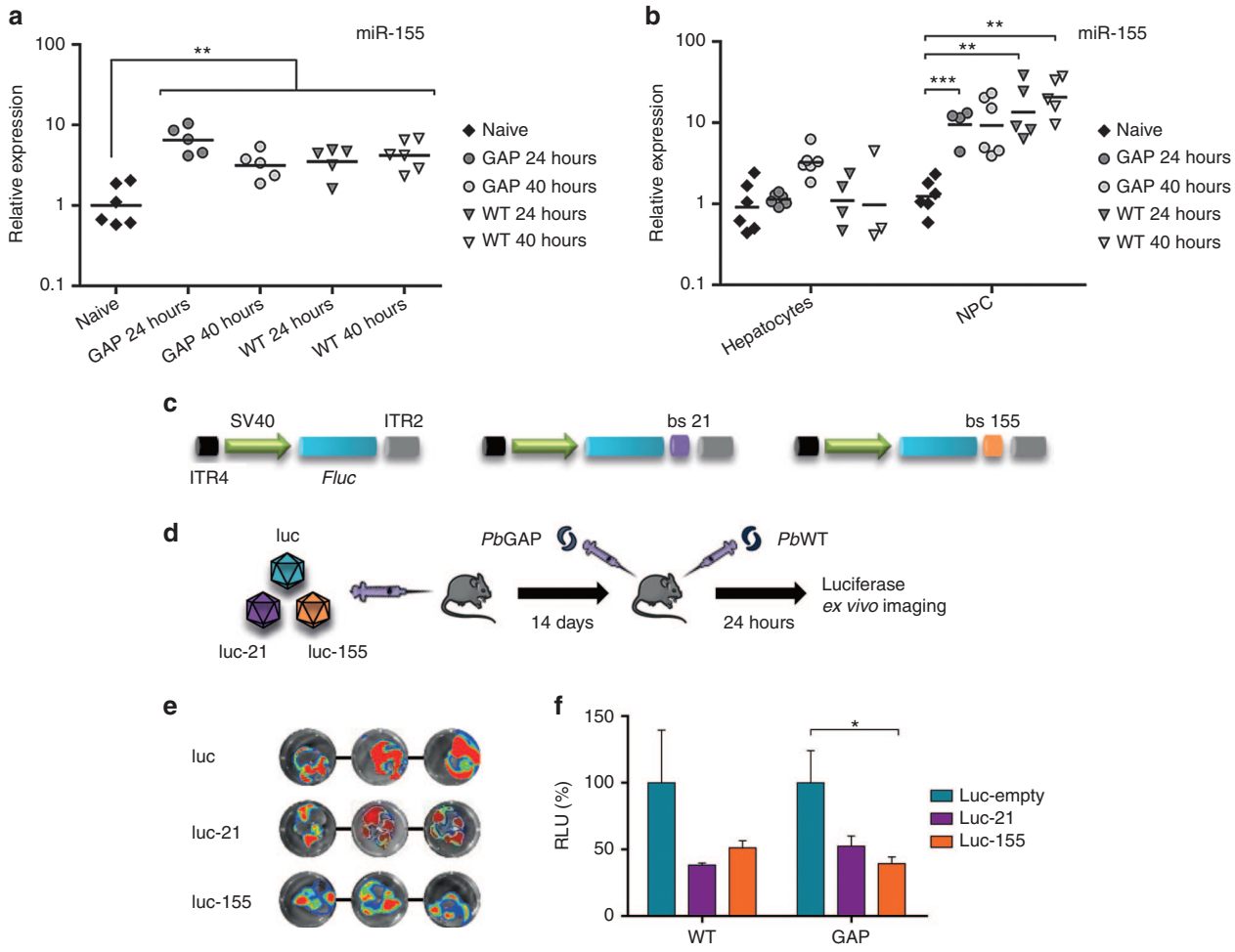

Figure 2 Identification of *in vivo* miR-155 dysregulation in *Plasmodium*-infected liver cells. (**a**) qRT-PCR-based detection of miR-155 in whole liver total RNA. Each symbol represents an individual mouse. $^{**}P < 0.01$ (one-way analysis of variance, Dunnett's test) (**b**) qRT-PCR-based detection of miR-155 in hepatocytes and non-parenchymal cells including Kupffer cells. Each symbol represents an individual mouse. $^{**}P < 0.01$, $^{***}P < 0.001$ (two-way analysis of variance, Bonferroni test) (**c**–**e**) *In vivo* validation of miR-21 and miR-155 increases in WT-/GAP-infected livers. (**c**) Reporter vectors to detect miR-21 or miR-155 expression. The Firefly *luciferase* gene was expressed from a SV40 promoter and tagged in its 3'UTR with a perfect binding site for miR-21 (center) or miR-155 (right), or none (positive control, left). Accordingly, in the presence of miR-21/-155, the corresponding luciferase reporter will be inhibited. ITR4/2, inverted terminal repeats (packaging signals) of AAV serotypes 4 or 2. (**d**) Injection scheme (each mouse received 2×10^{11} AAV reporter vectors). (**e**) Representative examples of livers from the mice in **d**. Colors indicate luciferase expression (blue: low, red: high). (**f**) Quantification of the data from **e**. Values were normalized to photon counts in livers of mice treated with the same luciferase vector without parasite infection, to eliminate miRNA-independent effects of the parasite on luciferase expression, and then to the respective luc-empty control. Luciferase values are inversely correlated with expression of the two miRNAs, *i.e.*, a miRNA increase will result in lower luciferase expression. RLU, relative light units (readout of the luciferase assay/software). $^{*}P < 0.05$ (two-way analysis of variance, Bonferroni test).

non-parenchymal cells including liver-resident macrophages (Kupffer cells) and T cells. In an effort to further narrow down the cell fraction(s) that contribute(s) to the miR-155 increase, we applied an alternative protocol for cell separation from whole livers from GAP-infected mice that included a different gradient (Nycodenz versus Percoll) as well as MACS-based specific enrichment of Kupffer as well as T cells (**Supplementary Figures S4–S5**). Notably, quantification of miR-155 in these new fractions that were now highly enriched for Kupffer or T cells, respectively (compare **Supplementary Figure S5c**), revealed the greatest increase relative to naïve mice in the Kupffer cells (**Figure 3e**). Milder, but also highly significant elevations of miR-155 were also seen in the hepatocyte and T-cell fractions. We thus conclude that GAP priming of mice triggers a broad miR-155 upregulation in several liver cell types, with the greatest effect seen in a fraction enriched in Kupffer cells.

Viral vectors for ectopic miR-155 dysregulation

Based on the sum of our findings, we hypothesized that deliberate ectopic upregulation of miR-155 may tip the balance between immune-augmenting (miR-155) and -suppressing (SOCS1, SHIP1 and others) factors and thus further boost the protective capacity of GAP parasites in mice. To test this hypothesis, we engineered viral gene transfer vectors based on adeno-associated virus serotype 8 (AAV8) to either encode a miR-155 expression cassette (under a ubiquitously active or a liver-tropic promoter), or an inhibitor of this miRNA (a "sponge," *i.e.*, multiple binding sites which sequester and inactivate miR-155) (**Figure 4a**). AAV8 was chosen as it potently infects hepatocytes as well as Kupffer cells in mice.[27,28] Indeed, we confirmed robust *in vivo* Kupffer cell infection by immunofluorescence using a GFP-encoding AAV8 and a specific macrophage marker (**Supplementary Figure S6a,b**),

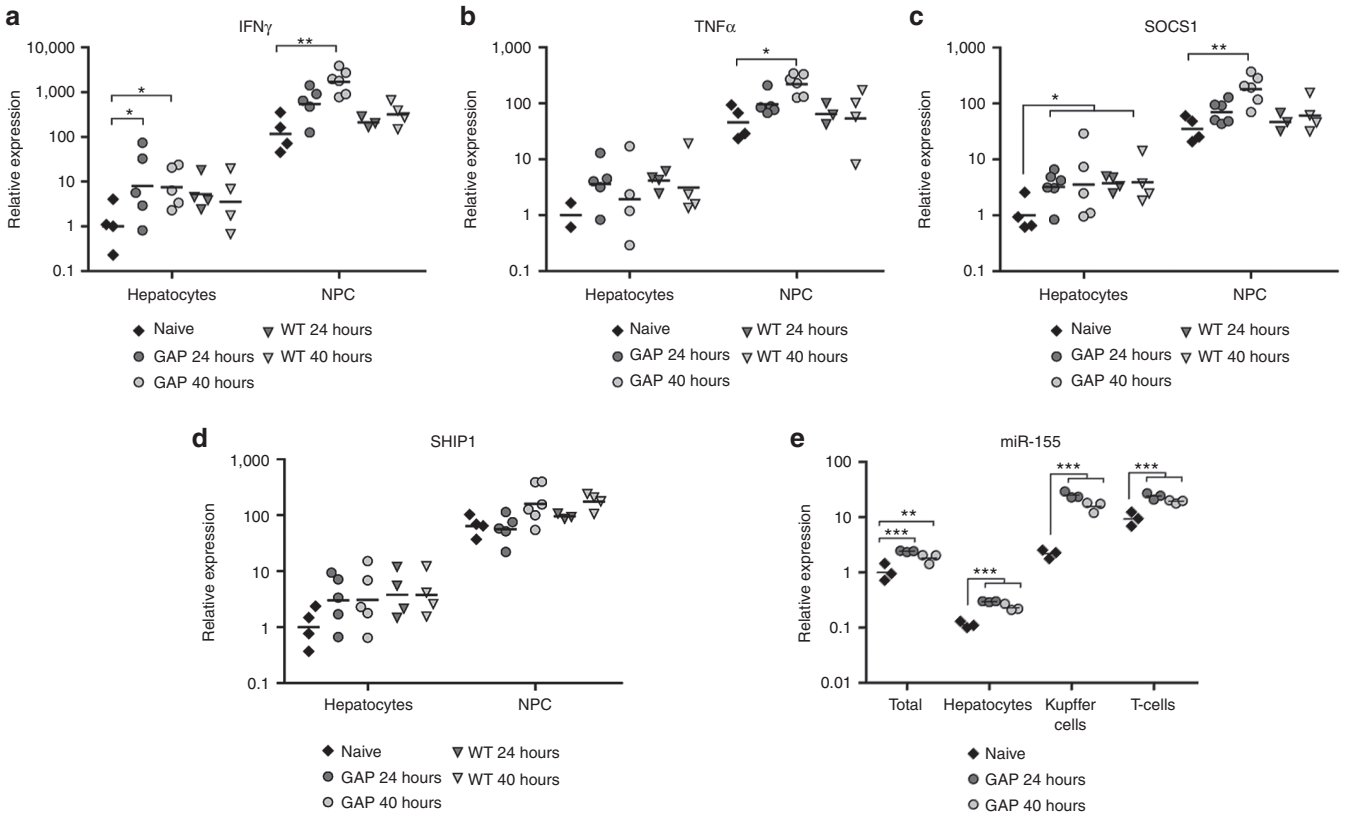

Figure 3 Analysis (qRT-PCR) of miR-155-related gene expression in hepatocytes versus non-parenchymal cells (NPC) of *Plasmodium*-infected mice. (**a**,**b**) Quantification of (**a**) IFNγ and (**b**) TNFα expression in naïve mice versus animals injected with GAP or WT parasites, measured at the indicated timepoints. All values are expressed relative to the naïve hepatocyte group which was set to 1. Each symbol represents an individual mouse. **P* < 0.5, ***P* < 0.01 (two-way analysis of variance, Bonferroni test) (**c**,**d**) Analogous quantification and depiction of (**c**) SOCS1 and (**d**) SHIP1 expression in the same mice from **a**,**b**. (**e**) Quantification of miR-155 expression in the indicated fractions and mouse cohorts using the stringent and specific cell separation protocol shown in **Supplementary Figures S4–S5**. All values are expressed relative to the naïve total liver group which was set to 1. Each symbol represents a pool of three mice. ***P* < 0.01, ****P* < 0.001 (two-way analysis of variance, Bonferroni test).

as well as by qRT-PCR-based detection of AAV8-mediated GFP or miR-155 expression (**Supplementary Figure S6c,d**). In addition, we verified the principal functionality of our vectors from Figure 4a through qRT-PCR analysis of miR-155 expression in total liver RNA from AAV-treated mice. As compared to naïve mice and negative controls, we were pleased to find a 2.5- (RSV promoter) to 1,000-fold (LP1 promoter) miR-155 upregulation in animals injected with the miR-155 overexpression vectors, and a 10-fold miR-155 inhibition in mice treated with the miR-155 sponge vector (**Supplementary Figure S6e,f**).

Effect of ectopic miR-155 inhibition

We first validated that animals vaccinated with our previously established prime-two boost immunization regime with GAP parasites remain sterily protected after infectious wild-type sporozoite challenge (Figure 4b,c and Table 1).[8] In contrast, animals that received only a single GAP priming, a regime never tested before, did not enjoy sterile protection, but instead showed only 77% immunity to infectious challenge (Figure 4b,c and Table 1). Salivary gland extracts from uninfected mosquitoes showed no effect (all mice became blood-stage-positive after wild-type challenge, Figure 4c and Table 1), proving that protection required GAP. Next, we injected 15 mice with the miR-155 sponge vector, followed 2 weeks later (to permit sponge expression and miR-155 inhibition) by a single GAP prime and a subsequent challenge with wild-type sporozoites after another week (Figure 4b). In parallel, we injected an equally large mouse group with an AAV8 vector without miRNA binding sites as a sponge control. From day 3 on after wild-type challenge, thin blood smears were taken to monitor the presence of parasite blood-stages and to determine prepatency (interval between infection and detection). We found that 6 out of 15 mice pretreated with the miR-155 sponge became blood-stage-positive (corresponding to 60% protection, 9/15 mice), while 11 out of 15 (73%) were protected in the sponge control group, similar to the numbers of mice that only received a single GAP shot (77%, Figure 4c and Table 1). These results indicated that vector-mediated miR-155 inhibition may alleviate the protective GAP effect in mice, but only partially. We therefore turned to a more stringent model and attempted to vaccinate miR-155 knock-out mice with GAP parasites, again followed by wild-type challenge 1 week later. In a control group that only received wild-type *P. berghei* NK65, six out of six mice (100%) became positive for intra-erythrocytic stages, proving that these knock-out mice were fully susceptible to parasite infection. Notably, five out of six mice in the group pretreated with GAP were protected (83%) against wild-type challenge, reminiscent of the 77% in regular mice. Collectively, the experiments with miR-155 sponge vectors and miR-155 knock-out mice suggest that, despite its increase

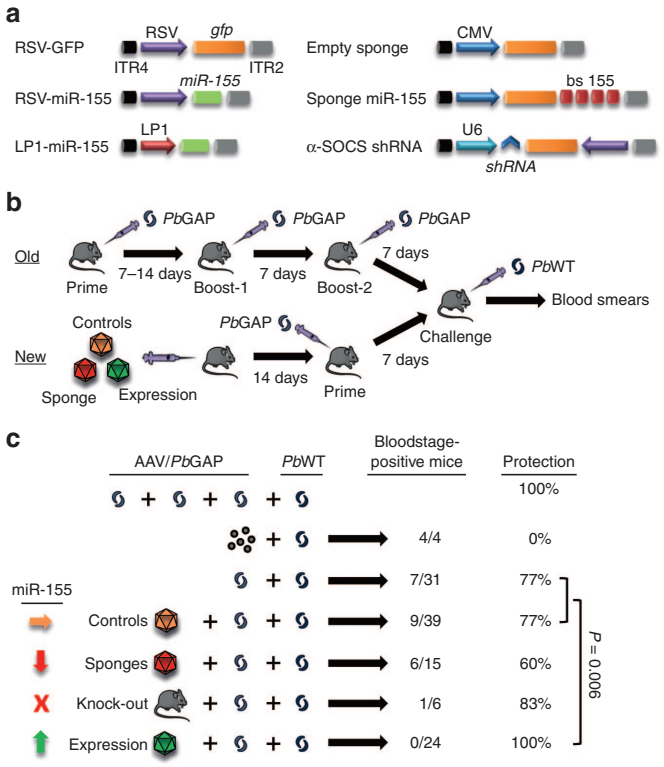

Figure 4 Ectopic miR-155 upregulation enhances GAP vaccination of mice against *Plasmodium*. (**a**) AAV vectors used in the experiments in this figure. Left: Vectors to express mouse miR-155 or *gfp* as control. Right: Vectors to inhibit miR-155 through expression of a sponge (*i.e.*, a CMV promoter-driven *gfp* cDNA with four imperfect miR-155 binding sites in its 3′UTR, middle), or to express an shRNA against mouse SOCS1 (bottom; this vector also encodes an RSV promoter-driven *gfp*). ITR4/2, inverted terminal repeats from AAV serotypes 2/4 (AAV replication and packaging signals). (**b**) Comparison of former (top) and improved (bottom) vaccination schemes. AAV vectors were applied at doses of 2×10^{11} particles per mouse. (**c**) Summary of the different vaccination regimes and results. The circles in the second line indicate "debris," *i.e.*, extracts from salivary glands from naïve mosquitoes. The *P* value was calculated using Fisher's exact test.

following GAP infection (**Figures 2a**,**b** and **3e**), miR-155 is not critically required for the protective GAP effect in mice but may rather enhance it.

Effect of ectopic miR-155 overexpression

Accordingly, we were interested in the reverse experiment where we wanted to further boost this potential enhancer function of miR-155, by upregulating it using our AAV8 vectors 2 weeks prior to one GAP prime and subsequent wild-type challenge (**Figure 4b**). AAV8 RSV-GFP and AAV8 RSV-miR-125b served as two internal controls (miR-125b was not dysregulated after GAP infection, **Supplementary Figure S2b**). Interestingly, the single-GAP–vaccinated group without any AAV8 was similar to the controls, with 77% protection from a single GAP prime, 75% with AAV8 RSV-GFP and 87.5% with AAV8 miR-125b, respectively (**Table 1**). Far more remarkable was, however, that pretreatment with the miR-155 overexpression vector significantly enhanced GAP vaccine potency and yielded 100% protection (0 of 24 mice became blood-stage-positive) (**Figure 4c** and **Table 1**). MiR-155 overexpression *per se* had no effect on WT parasite replication (100% (3/3) WT-infected mice became blood-stage-positive, regardless of prior miR-155 vector administration), proving that full protection required the combination of this miRNA with GAP. The only other group which showed the same high efficiency as the miR-155/GAP cohort was the established triple vaccination protocol, where mice had received two GAP boosts after the initial prime (**Table 1**).

Deliberate inhibition of miR-155 target SOCS1

Finally, we asked whether we could partially recapitulate the protection-enhancing effect of miR-155 overexpression by directly inhibiting one of its presumed targets *in vivo*, SOCS1. Indeed, pretreatment of mice with an AAV8 vector expressing a robust anti-SOCS1 short hairpin (sh)RNA (**Figure 4a** and **5a**,**b**), followed by a single GAP prime, also improved protection to 100% (versus only 43% with a control AAV8 expressing an irrelevant shRNA) (**Table 1**). While we do not interpret this result as a decisive proof that SOCS1 is the main miR-155 target in our scenario, it fits with the overall conclusion from our study that the potency of whole-organism malaria vaccines is determined by a fine balance between immune-stimulating and -suppressing factors in the host liver.

DISCUSSION

Here, we show that *in vivo* administration of attenuated malaria parasites rapidly and strongly induces a cascade of expression of pro-inflammatory host factors, including IFNγ, TNFα and miR-155. Intriguingly, upregulation of this specific miRNA was likewise reported in cells (including macrophages), animals and patients infected with various further pathogens, from bacteria and yeast, to other parasites and viruses.[26,29–34] Together with our present data, this supports the fundamental role of miR-155 in mammalian host defense mechanisms against pathogen challenge. Additional evidence comes from findings that miR-155-deficient mice cannot be vaccinated against *Salmonella*[35] or *Helicobacter*.[36] Interestingly, this is different for *Plasmodium* based on our observation of a partial ability of GAP to induce immunity in mice with reduced (AAV sponge-treated) or no (knock-out) miR-155. We thus conclude that miR-155 is not absolutely required for GAP protection, but that it plays an essential role in fine-tuning the strength of the immune response.

Mechanistically, our results in combination with previous studies imply that miR-155 negatively regulates (among others) a set of cellular immuno-suppressors (the miR-155 "targetome"),[35] providing a likely explanation how miR-155 upregulation might reinforce the anti-pathogen host response. This adds to our understanding of the very intricate and pleiotropic functions of miR-155 in the mammalian immune system, including the regulation of the germinal center response, the control of cytokine or antibody production, the augmentation of antiviral $CD8^+$ T-cell responses, or the promotion of the development of inflammatory IL-17–producing Th17 cells, to name a few.[29,35,37–40]

The findings presented here not only shed further light on the *in vivo* role of this miRNA and on *Plasmodium* intrahepatic biology, but likely also bear clinical relevance. This is exemplified by a recent study showing that up to five repeated RAS injections are required to trigger protective immunity in human adults.[10] In

Table 1 Vaccination enhancement through miR-155 upregulation or target downregulation

Immunization (AAV8/*uis3*(-) sporozoites)	Boost(s) with attenuated sporozoites (number/day)	Challenge with wild-type sporozoites (number/day)	Number of protected/ challenged mice	Degree of protection
–/10,000	#1: 10,000/d 14	10,000/d 28	5/5	100%
	#2: 10,000/d 21			
–/–	–/–	10,000	0/5	0%
–/10,000	#1: 10,000/d 7	10,000/d 21	5/5	100%
	#2: 10,000/d 14			
–/–	–/–	10,000	0/5	0%
–/10,000	–/–	10,000/d 7	24/3	77%
–/–	–/–	10,000	1/33	0.05%
RSV-GFP/10,000	–/–	10,000/d 7	12/16	75%
RSV-miR-125b/10,000	–/–	10,000/d 7	7/8	87.5%
RSV-miR-155/10,000	–/–	10,000/d 7	11/11	100%
LP1-miR-155/10,000	–/–	10,000/d 7	13/13	100%
miR-155 sponge/10,000	–/–	10,000/d 7	9/15	60%
Sponge control/10,000	–/–	10,000/d 7	11/15	73%
Anti-SOCS1 shRNA/10,000	–/–	10,000/d 7	8/8	100%
shRNA control/10,000	–/–	10,000/d 7	3/8	37.5%
–/–	–/–	10,000/d 7	0/8	0%

C57BL/6J mice were intravenously injected with the indicated AAV8 vectors (left column): sponges against miR-155 or empty sponge, constructs overexpressing miR-155 (under a ubiquitous RSV or a liver-tropic LP1 promoter), or miR-125b or GFP as controls, or vectors expressing a specific shRNA against murine SOCS1 (or an irrelevant control shRNA). Fourteen days later, the same mice were intravenously injected (primed) with 10,000 *Pb*GAP sporozoites, and 7 days later challenged with 10,000 *Pb*NK65 sporozoites intravenously. Presence of parasites in the blood of the mice was monitored by daily blood smears from day 3 postinjection onwards.

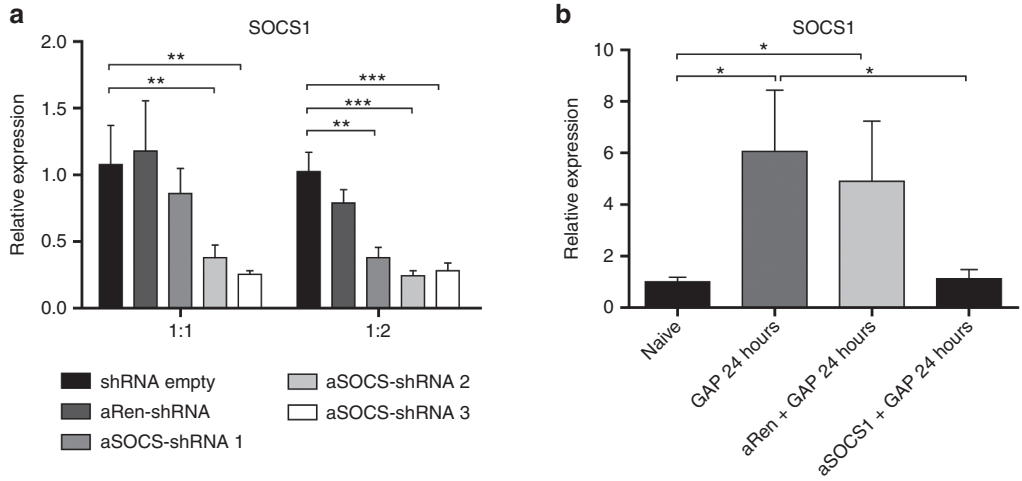

Figure 5 Function of potent anti-SOCS1 shRNAs *in vitro* and *in vivo*. (**a**) Constructs encoding three different shRNAs against murine SOCS1 under a U6 promoter and a plasmid expressing murine SOCS1 were co-transfected into HEK293T cells. Negative controls were the parental vector (empty) or a construct encoding an shRNA against *Renilla* luciferase (αRen). Numbers at the bottom indicate ratios of shRNA and SOCS1 plasmid. Total mRNA was isolated 48 hours posttransfection, and SOCS1 mRNA levels were quantified by qRT-PCR and normalized to the empty vector control (set to 1). αSOCS shRNA #3 was selected as the most potent shRNA for further experiments. Values are means of three independent transfections (±SD). (**b**) *In vivo* validation of the selected anti-SOCS1 shRNA from **a**. Mice ($n = 3$) were infused with the shRNA-expressing AAV8 vector (or an irrelevant control shRNA, αRen) at a dose of 5×10^{10} particles per mouse and 2 weeks later injected with GAP parasites. Consistent with all other data, GAP infection caused an increase in SOCS1 (detected 24 hours later), which was potently and significantly counteracted by the specific anti-SOCS1 shRNA vector (rightmost bar). *$P < 0.05$; **$P < 0.01$; ***$P < 0.001$ (one-way analysis of variance, Dunnett's test).

contrast, our work suggests the feasibility to also achieve complete sterile immunity from a simpler and faster dual AAV-GAP regime, which could especially benefit remote rural areas where patient access and compliance are critical. Concurrently, by replacing two GAP administrations in the original triple-shot protocol with a single AAV dose, our new regime may also alleviate a central technical bottleneck in the use of attenuated parasites as vaccines, which is their large-scale preparation under standardized conditions (the latter are established for AAV which has recently been commercialized as gene therapy drug in Europe). Considering

that our present work predominantly focused on primary vaccine/immune responses, it will now be an interesting goal for follow-up studies to determine whether miR-155 can also boost the long-term vaccination potential of GAP.

Important to note is that ectopic interference with an endogenous miRNA, such as miR-155 overexpression here, always includes a risk of unintentional adverse effects. In fact, miR-155 is naturally increased in many tumors and autoimmune diseases, suggesting a role as oncomir and making miR-155 inhibition rather than overexpression beneficial in these cases.[17,29,41–45] Others, however, reported evidence that blocking miR-155 might result in a loss of important functions, such as in tumor immunosurveillance,[46] eradication of bacterial infections,[47] or protection from hepatosteatosis.[48] Here, we observed no toxicity or liver tumorigenesis in our mice for up to 4 months after AAV8/miR-155 infusion. Evidence was that there were no gross pathologies, *i.e.*, no loss of weight or appetite, no behavioral abnormalities as well as no obvious changes in color and morphology of the liver (or any other organ) when we sacrificed the animals. Moreover, liver transaminases (markers for liver damage) in the serum of these mice were normal or only marginally elevated (AST: 91–176 U/l, ALT: 35–47 U/l (normal is up to about 50 U/l in both cases)). Still, we cannot rule out that sustained *in vivo* miR-155 overexpression may have adverse long-term effects. We therefore consider it essential in the future to better dissect the molecular targets and cellular pathways controlled by miR-155 in the liver and other tissues, to identify further means for ectopic modulation of the host immune system, such as already exemplified here with direct suppression of SOCS1. Alternatively or in addition, it should be highly rewarding to create and use AAV vectors that express miR-155 from an inducible promoter, which would allow maximum temporal control over miR-155 overexpression and in turn a reduction of potential adverse events.

Concurrently, it will also be important to further fine-tune the cellular specificity of the miR-155–expressing vectors, to additionally increase the stringency and safety of the approach. Interesting in this context is our observation that the vector with the LP1 promoter was also capable of boosting the GAP vaccine, considering that this promoter is believed to be specific for hepatocytes. In line with this, we also noted an increase in endogenous miR-155 in the hepatocyte fraction of livers from GAP-treated mice (**Figure 3e**). Moreover, miR-155 was also elevated in the T-cell fraction of these mice, yet the increase in the Kupffer cell fraction was clearly most pronounced. One possible explanation is that miR-155 is predominantly upregulated in Kupffer cells of GAP-treated mice, and is then secreted and transported to other liver cell types. Although our data in **Supplementary Figure 2c** argue against trafficking of miR-155 through the blood of *Plasmodium*-infected animals, one route may be direct cell-to-cell transfer of miRNAs which has in fact been reported in the liver.[49] *Vice versa*, this may explain why and how also the LP1-driven miR-155 expression vector enhanced the GAP vaccine, as the substantial, 1,000-fold miR-155 upregulation that we measured for this construct (**Supplementary Figure 6e**) may have resulted in miR-155 transfer to neighboring Kupffer cells. Alternatively, it is of course well conceivable that following GAP injection, miR-155 concomitantly increases to different extents in multiple cell populations in the liver and exerts pleiotropic functions in each that synergize or are partially redundant. This could again explain why both, the ubiquitous RSV- and the hepatocyte-specific LP1-miR-155 vector, were capable of enhancing the GAP vaccine. It is thus an intriguing and important goal for future work to create and test miR-155-expressing AAV vectors with other highly cell type-specific promoters, not only to further improve the safety of the approach, but also to shed additional light on the biological mechanisms underlying our observations. Finally, it may also be beneficial and safe to use miR-155 mimics, *i.e.*, "naked" RNA molecules resembling mature miR-155 in structure and function that typically only act transiently, which would likewise help to minimize potential risks.

Recently, a number of seminal (pre-) clinical studies have highlighted the tremendous potential of deliberate miRNA modulation as a novel biotherapeutical modality, including the use of miR-26a–expressing AAV8 to suppress hepatocarcinogenesis in mice,[50] or of miR-122 inhibitors to reduce Hepatitis C viral loads in chronically infected humans.[51] The present work adds the exploitation of mammalian miR-155 as a vaccine enhancer to this growing list of medically relevant original miRNA applications. As our strategy is largely compatible with the continuously improving viral and non-viral *in vivo* gene delivery tools, it has great potential to foster the development of new generations of better, simpler and safer vaccine formulations not only against malaria, but also numerous other infectious diseases.

MATERIALS AND METHODS

Cell culture. HEK293T cells were maintained and grown in Dulbecco's modified Eagle's medium (DMEM; Life Technologies, Carlsbad, CA) supplemented with 10% fetal calf serum (Biochrom AG, Berlin, Germany), 200 µmol/l L-glutamine and penicillin-streptomycin (both Life Technologies). Plasmid DNA transfections were carried out in 24-well plates, using Lipofectamine 2000 (Life Technologies) and following the manufacturer's instructions for this format.

Plasmids and AAV vector constructs. To generate luciferase-based miRNA reporter AAV vectors, binding sites for murine miR-21 and miR-155 were inserted into the 3′ untranslated region (UTR) of Firefly luciferase within a self-complementary AAV vector plasmid.[28] Binding sites were generated by annealing oligonucleotides miR-21 for 5′-TCG AGT CAA CAT CAG GAC ATA AGC TAT CTA GAG C-3′ and miR21-rev 5′-GGC CGC TCT AGA TAG CTT ATG TCC TGA TGT TGA C-3, or miR-155 for 5′-TCG AGA CCC CTA TCA CGT CAA GCA TTA ATC TAG AGC-3′ and miR-155 rev 5′-GGC CGC TCT AGA TTA ATG CTT GAC GTG ATA GGG GTC-3′, respectively. To create AAV/miRNA sponge constructs,[52] concatamerized imperfect miR-155 binding sites were inserted into the 3′UTR of a CMV promoter-driven *gfp* gene within a self-complementary AAV vector plasmid.[53] To obtain plasmids overexpressing miR-155, 258 bp comprising the miR-155 stem-hairpin were PCR-amplified from the *M. musculus* genome using the primer pairs RSVfor 5′-CGT AGT GGA TCC CAA ACC AGG AAG GGG AAG TGT G-3′ and RSVrev 5′-GAG TCG GCT AGC CAT CCA GCA GGG TGA CTC TTG G-3′, or LPfor 5′-CGT AGT GAA TTC CAA ACC AGG AAG GGG AAG TGT G-3′ and LPrev 5′-GAC TCG CTC GAG CAT CCA GCA GGG TGA CTC TTG G-3′ for cloning of the miR-155 coding sequence under an RSV or LP1 promoter, respectively. PCR products were *BamHI*/*NheI* (RSV) or *EcoRI*/*XhoI* (LP1) digested and then ligated into appropriately digested self-complementary AAV plasmid backbones[28] containing the RSV or LP1 promoters. A control plasmid expressing miR-125 was cloned in an identical manner, using the primers 125 for 5′-CGT AGT GGA TCC CTT ATG TTT CTG TCT GTG TGT TTC-3′ and 125 rev 5′-GAC TCG GCT AGC TTG TCA TGG

TGA AAC CCT TGC TG-3′. Self-complementary AAV vectors expressing shRNAs against murine SOCS1 under a U6 promoter were generated using our previously published shRNA cloning strategy.[28] Targeted sense sequences (selected via http://www.sirnawizard.com) were 5′-AGA TCT GGA AGG GGA AGG AAC-3′, 5′-CAA TAG AAG CCG CAG GCG TCC-3′ or 5′-GGA GAT CGC ATT GTC GGC TGC-3′ for shRNAs 1 to 3, respectively. A control AAV vector expressing an anti-luciferase shRNA was published.[54] A plasmid expressing murine SOCS1 from a CMV promoter was a kind gift of Alexander Dalpke (Heidelberg University Hospital, Germany).

AAV production. AAV vector particles expressing luciferase reporters, miRNA coding sequences, miR-155 sponges or anti-SOCS1 shRNAs were produced using a recently published triple transfection protocol[55] and purified via cesium chloride density gradient centrifugation.[28]

RNA isolation. For RNA isolation from total liver, frozen liver pieces were homogenized in 1–2 ml QIAzol reagent (Qiagen, Hilden, Germany) using a TissueRuptor (Qiagen). RNA was subsequently isolated according to the manufacturer's manual and resuspended in an appropriate volume of nuclease-free water (Life Technologies). Integrity of RNA was determined by measuring the RNA integrity number (RIN) of the samples with an Agilent 2100 Bioanalyzer and 2100 expert Eukaryote Total RNA nano chips (Agilent Technologies, Santa Clara, CA). The amount of small RNAs within the samples was determined by running Small RNA Series II chips (Agilent Technologies). For hepatocyte and NPC RNA isolation, cell pellets were resuspended in 1 ml Qiazol and purified the same way. RNA was isolated from hepatocytes as well as MACS-sorted Kupffer cells and T cells using a miRNeasy kit (Qiagen) following the manufacturer's instructions, including an on-column DNase I digestion.

miRNA labeling and detection by microarrays. Three µg of total RNA per sample were labeled using Exiqon miRCURY LNA microRNA Array Power Labeling Kit (Exiqon, Vedbaek, Denmark) according to the manufacturer's protocol. Naïve samples were labeled with Hy3 and experimental samples with Hy5. Spike-in controls were from the miRXplore Microarray Kit (Miltenyi Biotec, Bergisch-Gladbach, Germany). Hybridization to Miltenyi miRXplore microarrays 5.0 (Miltenyi Biotec) was performed overnight by using the miRXplore Microarray Kit (Miltenyi Biotec) according to the manufacturer's manual and an a-Hyb Hybridization Station (Miltenyi Biotec). Hybridized microarrays were then analyzed with a Scanarray 4000 XL (Packard Biochip Technologies, Billerica, MA). Raw data collection was performed using GenePix Pro 6 software (Axon Instruments/Molecular Devices, Sunnyvale, CA) with an optimal setting of Cy3 and Cy5 channels. Raw data were then processed using the R language (project.org) and the "limma" (Linear Models for Microarray) package from the Bioconductor project (http://www.bioconductor.org/). The means of the pixel distribution for the foreground and background signal were used as estimators of the raw signal values in both channels. By dividing foreground through background intensities, we calculated signal-to-noise ratios (SNR). Spots that had been automatically flagged during the scanning process with Genepix and that have an SNR <1 were weighted with only 10% in the following analyses. Next, data were normalized using loess normalization on the normexp-background corrected signal intensities. Thereafter, a Gquantile normalization was used to normalize all expression values against the naïve control in the Cy3 channel of each microarray. All methods were used as provided in the limma package. Furthermore, we computed for each spot the log fold-change (fc) of the samples with the different parasites and treatments versus the naïve samples without parasites. The fc values of the biological replicates (three replicates for 24 hours and two replicates for 40–44 hours), have been summarized taking the average. Differentially expressed miRNAs were calculated by applying the Welch one-sample *t*-test on the summarized fc as implemented in R. We applied a Bonferroni *P* value correction to account for multiple testing. We furthermore filtered out miRNAs which have a SNR <1.2.

Validation of miRNAs. Individual miRNAs were validated with qRT-PCR, using predesigned miScript Primer Assays and miScript SYBR Green PCR Kit in a Corbett RotorGene 6000 PCR cycler (all Qiagen). Prior to qRT-PCR, RNAs were DNase-treated using Turbo DNA Free Kit (Ambion) before 1 µg total RNA was transcribed to cDNA of miRNAs using miScript Reverse Transcription Kit (Qiagen). Per qPCR reaction, 3 ng cDNA were added to a final reaction volume of 15 µl. Cycling conditions were as follows: 15 minutes initial activation step at 95 °C, followed by 45 cycles with 15 seconds denaturation at 94 °C, 35 seconds annealing at 55 °C and 30 seconds extension at 70 °C. During the extension step, fluorescence was measured.

Quantification of miR-155 regulators and target genes. Reverse transcription of 2.5 µg total DNase-digested RNA was performed using the Tetro cDNA Synthesis Kit (Bioline, London, UK) according to the manufacturer's instructions. cDNA of total liver RNA was diluted 1:5 in water for the detection of TNFα, and 1:15 for the detection of IFNγ. cDNA of RNA purified from separated hepatocytes and non-parenchymal cell fraction was diluted 1:2 in water. One qPCR reaction consisted of 2 µl cDNA, 7.5 µl SensiMix Sybr No-Rox Mastermix (Bioline), 0.375 µl of each primer (10 mmol/l) and 4.75 µl water. Quantitative PCR was performed on a Qiagen Rotor-Gene 6000 using 45 cycles of 95 °C, 60 °C and 72 °C (15 seconds each), with subsequent melting curve analysis to verify correct amplification. Relative expression levels were calculated according to the ΔΔCt method. GAPDH served as housekeeper. The following primers were used: GAPDH forward 5′-TTG ATG GCA ACA ATC TCC AC-3′ and reverse 5′-CGT CCC GTA GAC AAA ATG GT-3′, TNFα forward 5′-AAA ATT CGA GTG ACA AGC CTG TAG-3′ and reverse 5′-CCC TTG AAG AGA ACC TGG GAG TAG-3′, IFNγ forward 5′-TGC CTC TGC AGG ATT TTC ATG-3′ and reverse 5′-TCA AGT GGC ATA GAT GTG GAA GAA-3′, SHIP1 forward 5′-GAG CGG GAT GAA TCC AGT GG-3′ and reverse 5′-GGA CCT CGG TTG GCA ATG TA-3′, SOCS1 forward 5′-ACA GTC GCC AAC GGA ACT G-3′ and reverse 5′-GGG CCC GAA GCC ATC TT-3′. The significance of the difference in gene expression in the treated groups compared to the naive control was assessed using a one-way analysis of variance test with Dunnett's test in measurements of total liver, and using a two-way analysis of variance test followed by a Bonferroni test in measurements involving specific fractions of the liver cells.

cDNA profiling and pathway analyses. Mouse Sentrix-6 Whole Genome Expression BeadChips (Illumina, San Diego, CA) were used to identify genes expressed in *Plasmodium*-infected (*Pbuis3(-)*, *Pb*NK65) versus non-infected hepatic tissue. First/second strand cDNA synthesis as well as chip hybridization and chip scanning were essentially performed as described recently.[55] Raw data were exported from the Beadstudio software to R, and then quantile normalized and log2 transformed. Pathway analyses were conducted using Metacore (thomsonreuters.com/metacore/) and Ingenuity (IPA, http://www.ingenuity.com) software.

Isolation and analysis of exosome-associated miRNAs by qPCR. Exosomes were isolated from mouse serum using Total Exosome Isolation reagent (Life Technologies) according to the manufacturer's instructions. Briefly, 10 µl of Exosome Isolation reagent were added to 50 µl mouse serum, and samples were incubated for 30 minutes on ice. Next, samples were centrifuged (10,000*g*, 10 minutes at 25 °C), and the resulting exosome-containing pellets were dissolved in 500 µl Trizol (Life Technologies) by incubating at 65 °C for 5 minutes. Exosomal RNAs were extracted using the miRNeasy kit (Qiagen) and eluted into 50 µl RNase-free water. Expression levels of exosomal miRNAs were determined using miQPCR, a unique PCR strategy that relies on the universal reverse transcription of all miRNAs contained in an RNA sample.[56] Therefore, 4 µl RNA were reverse-transcribed via miQPCR. Resulting cDNAs were diluted to 250 µl, of which 2.5 µl were used in the qPCR. The qPCR reactions were carried out on a Viia7 qPCR cycler (Life Technologies), and amplicons were detected using SYBR green

I (Life Technologies). Relative miRNA expression levels were calculated using qBASE[57] and the ΔΔCt method.

***Plasmodium* work including vaccinations.** Frozen blood stocks of *Plasmodium berghei* NK65WT and *uis3(-)* parasites[8] were injected into naïve NMRI mice and, once enriched for gametocytes, subsequently fed to female *Anopheles stephensi* mosquitoes. At day 17–21 postinfection, salivary glands of female mosquitoes were dissected to isolate sporozoites. For infection of C57BL/6J mice, groups of six mice each were injected intravenously with 50,000 or 10,000 *Pb*NK65 WT, RAS and *uis3*(-) sporozoites per mouse (respective sporozoite numbers are mentioned in the text and the figures). *P. berghei* NK65 WT sporozoites were γ-irradiated on ice with a dose of 150 gray resulting in radiation-attenuated sporozoites (RAS).[7] Twenty-four and 40–44 hours postinjection, three mice per group were sacrificed and PBS-perfused via heart puncture. Small pieces of liver were resected, flash-frozen in liquid nitrogen, transferred into nitrogen-cooled 2 ml microcentrifuge tubes and immediately stored at −80 °C. For experimental vaccination studies, female C57BL/6J mice were injected intravenously with AAV vectors (5×10^{10} for AAV8-anti-SOCS1 shRNA and AAV8-shRNA control; 2×10^{11} particles per animal for all other vectors). Fourteen days later, mice were primed intravenously with 10,000 *Pbuis3(-)* sporozoites and subsequently challenged with 10,000 infectious NK65 sporozoites 7 days later. In parallel, one group of mice received *Pbuis3(-)* sporozoites without prior AAV injection, and naïve animals served as control. As a control vaccination regime, a prime-boost-boost protocol was applied as described previously.[8] Briefly, female C57BL/6J mice were primed with 10,000 *Pbuis3(-)* sporozoites followed by one or two booster injections either day 7/14 or day 14/21 postpriming (10,000 *Pbuis3(-)* sporozoites each). Immunized mice were subsequently challenged after the final booster injection with 10,000 infectious *Pb*NK65 wild-type sporozoites (as indicated in **Table 1**). Naïve mice and mice solely infected with non-infectious salivary glands of *Anopheles* mosquitoes served as controls.

Mice. C57BL/6J or NMRI mice were purchased from Janvier (Saint Berthevin Cedex, France) and kept under specified pathogen-free conditions in the animal facility at Heidelberg University (IBF). C57BL/6J mice with a knock-out of miR-155 (strain B6.Cg-Mir155$^{tm1.1Rsky}$/J) were purchased from The Jackson Laboratory (Bar Harbor, ME) and kept under the same conditions. All animal experiments were performed according to European regulations and approved by the state authorities (Regierungspräsidium Karlsruhe, Germany). For *ex vivo* luciferase imaging, livers were removed from mice 24 hours after intravenous injection with 10,000 *Plasmodium berghei* WT or GAP parasites, respectively, and placed in 1× PBS in a six-well plate. D-Luciferin (Synchem, Felsberg, Germany) was then added and luciferase activity measured within 10 minutes using an IVIS-100 camera (Caliper/Perkin-Elmer, Waltham, MA).

Kupffer cell and cholangiocyte staining. Adult male C57BL/6J mice were injected intraperitoneally with 0.5 µl/g body weight CCl_4 diluted 4× in corn oil (both Sigma-Aldrich, St Louis, MO) twice weekly for 8 weeks. Each mouse received 4×10^{11} viral genomes of AAV8 vector expressing EYFP from the CMV promoter by tail vein injection. This dose is two-fold higher than the dose used in all other experiments (2×10^{11}) to ensure efficient YFP detection by immunofluorescence; for the same reason, we used a strong CMV promoter in these vectors. Mice were killed for analysis 2 weeks after vector injection. Liver samples were fixed overnight in zinc formalin (Anatech, Battle Creek, MI), embedded in paraffin, cut into 5-µm-thick sections, and placed on Superfrost Plus slides (Fisher Scientific, Pittsburgh, PA). Sections were deparaffinized and boiled in Antigen Retrieval Citra Solution (BioGenex, Fremont, CA) for 10 minutes. After blocking in 10% donkey serum for 1 hour, sections were incubated with 1/200 dilutions of the primary antibodies chicken anti-GFP (Abcam, Cambridge, UK), rat anti-F4/80 (Serotec, Oxford, UK) or rabbit anti-CK19 (AbboMax, San Jose, CA) overnight at 4 °C, and 1/200 dilutions of the secondary antibodies donkey anti-chicken-DyLight 549, donkey anti-rat-DyLight 488 or donkey anti-rabbit DyLight 488 for 1 hour at room temperature. Nuclear DNA was stained with 300 nmol/l DAPI (Millipore, Billerica, MA).

Determination of liver inflammation. To determine the level of ALT (alanine aminotransferase), AST (aspartate aminotransferase) and hemolysis from mice injected with AAV8 vectors and vaccinated with *Pbuis3(-)* sporozoites, serum was taken 56 days after AAV/miR-155 vector injection and processed by the Heidelberg University Hospital Analysezentrum.

Isolation and purification of primary hepatocytes and non-parenchymal cells using Percoll gradients. Primary hepatocytes were separated from the remaining liver cells of either naïve mice or mice infected with *P. berghei* liver-stages. Prior to the procedure, buffers were heated to 42 °C for perfusion, and tubes and catheters were filled with buffers to avoid the occurrence of air bubbles. Buffers were kept at 42 °C in a water bath during the whole procedure. Mice were sacrificed, and the abdomen was opened by cutting through the skin and abdominal wall without injuring the liver and the intestines. *Vena cava* and portal vein were exposed by shifting the intestines, and a vein catheter was carefully inserted into the *Vena cava inferior*. Following a cut of the portal vein, the liver was perfused for 5 minutes with 1× EGTA buffer (2 mmol/l glutamine, 0.5% glucose, 25 mmol/l HEPES, 2 mmol/l EGTA, pH 7.4) using a peristaltic pump (using a flow rate of 5–8 ml/minute), followed by 10 minutes perfusion with 1× collagenase solution (2 mmol/l glutamine, 0.5% glucose, 25 mmol/l HEPES, 3 mmol/l $CaCl_2$, pH 7.4, supplemented with 0.3 mg/ml collagenase (Gibco/Life Technologies)). Afterwards, the liver was cautiously removed from the abdomen and kept in a petri dish with HBSS buffer (Life Technologies). Connective tissue around the liver was carefully pulled off to release the cells. The suspension was pipetted several times to singularize cells, followed by filtering through a 100 µm cell strainer. Petri dish and cell strainer were washed with 5–10 ml HBSS buffer, which was then combined with the suspension in a 50 ml polypropylene tube and centrifuged for 5 minutes at 27*g* and 4 °C. The resulting supernatant was used for the isolation of the non-parenchymal cell fraction, whereas the pellet was used to purify hepatocytes as recently described.[58] The pellet was resuspended in 19 ml Percoll (9.748 ml Percoll (1.124 g/ml, Biochrom AG), 10.252 ml HBSS) and centrifuged for 10 minutes at 62*g* and 4 °C, without brake. The cell pellet containing hepatocytes was immediately resuspended in 10 ml HBSS buffer and pelleted once as a washing step. For further analysis the hepatocyte fraction was ultimately resuspended in 1 ml QIAzol (Qiagen) and transferred to nuclease-free Eppendorf tubes. To obtain the non-parenchymal cell fraction, the supernatant was pelleted at 625*g* and 4 °C for 7 minutes. The resulting pellet fraction was then resuspended in 6 ml HBSS buffer and placed on a 50%/25% two-step Percoll gradient before centrifugation. After centrifugation, the cells were separated into four fractions of which the two middle fractions represent the non-parenchymal cell fractions. These two fractions were combined and washed once in HBSS buffer, and after pelleting resuspended in 1 ml QIAzol (Qiagen) and transferred to nuclease-free Eppendorf tubes. Prior to resuspension of both the hepatocytic and non-parenchymal fraction, a viability test by Trypan Blue staining (Sigma) was carried out. All resuspended cells were stored at −80 °C.

Isolation and purification of primary hepatocytes, Kupffer cells and T cells via Nycodenz gradient and MACS. Naïve, *Plasmodium*-infected or AAV-injected mice were sacrificed via CO_2 and opened up, and the portal vein and *Vena cava* were exposed as described above. Livers were perfused via the portal vein first with SC-1 solution, followed by Pronase E solution (33 mg Pronase E (Roche, Mannheim, Germany) per 100 ml SC-2 buffer) and by collagenase solution (20500 U collagenase CLS4 (Worthington, Lakewood, NJ) per 100 ml SC-2 buffer). The composition of all buffers used for cell separation is listed in **Supplementary Table S6**. All buffers were adjusted to a pH of 7.2–7.3 and stored at 4 °C until use. All perfusions were performed for 6 minutes 30 seconds at a flow rate of ~2 ml/minute, using buffers that were prewarmed to 40 °C. Per cell isolation, livers of three mice were removed, pooled and digested for

another 30 minutes at 37 °C in 100 ml collagenase/pronase/DNase solution (25 mg pronase E, 7750 U collagenase and 1 mg DNase (Roche) in 100 ml SC-2 buffer). Liver cells were brought into suspension by gently tearing the livers using a 10 ml pipet, and were then filtered through a 70 µm cell strainer. Hepatocytes were separated via 1 minute centrifugation at 500 rpm and the pellet was further purified as described above. The non-parenchymal cells in the supernatant were pelleted for 8 minutes at 750*g*, washed once with 20 ml GBSS/B containing 0.6 mg DNase and resuspended in a final volume of 34 ml GBSS/B containing 0.3 mg DNase. 14 ml Nycodenz solution (5,18 g Nycodenz (Axis-Shield, Oslo, Norway) in 15 ml GBSS/A) were added and two gradients were prepared by layering 25 ml of cells on top of 12 ml Nycodenz 2 solution (3.63 g Nycodenz in 25 ml GBSS/A). The gradients were topped with 3 ml GBSS/B and centrifuged for 20 minutes at 1,690*g* without brake. The interlayer containing non-parenchymal cells was collected and washed with GBSS/B. For removal of erythrocytes, the pellet was resuspended in 3 ml erythrocyte lysis buffer and incubated for 5 minutes on ice. After addition of 7 ml GBSS/B, cells were pelleted for 5 minutes at 1,100 rpm, washed once with 10 ml GBSS/B and resuspended in 500 µl GBSS/B. To block unspecific antibody binding, 7.5 µl Fc receptor block was added and incubated for 5 minutes on ice, before staining Kupffer cells with a PE-coupled anti-F4/80 antibody (eBiosciences, Frankfurt, Germany) for another 30 minutes on ice. Cells were washed with 1 ml PBS and centrifuged for 5 minutes at 4 °C and 500*g*. The pellet was resuspended in 80 µl MACS buffer per 10^7 cells (PBS/0.5% BSA/2 mmol/l EDTA) and stained for 15 minutes with αPE-Beads (Miltenyi) according to the manufacturer's instructions. Kupffer cells were separated using a Vario MACS and LS Columns (Miltenyi) according to the manufacturer's instruction and eluted in 5 ml MACS buffer. The flow through (flow through 1) was collected for flow cytometry analysis and T-cell staining. Both cell fractions were counted and pelleted for 5 minutes at 1,100 rpm. The Kupffer cell pellet was resuspended in 700 µl Qiazol and stored at −80 °C until RNA isolation. T cells were purified from the flow through 1 in the same manner as described above for Kupffer cells, using 10 µl αCD5 beads (Miltenyi) and eluted in 5 ml MACS buffer. The flow through 2 was collected as well for flow cytometry. T cells were pelleted, resuspended in 700 µl Qiazol and stored at −80 °C.

Flow cytometry analysis of cell types in fractionated livers. The non-parenchymal cell fraction was analyzed by Flow cytometry using anti-mouse CD90.2-FITC (eBioscienes, clone 30-H12) and anti-mouse F4/80-PE (kindly provided by Adelheid Cerwenka, DKFZ, Heidelberg, Germany). Staining was performed for 20 minutes on ice followed by one washing step with PBS (Life Technologies). Cells were measured with a FACS Calibur (Becton Dickinson GmbH) and further analyzed using the BD CellQuest Pro Software (Version 6.0). Hepatocytes, Kupffer cells and T cells as well as the respective flow through fractions were analyzed by flow cytometry after staining of ~10^5–10^6 cells of each fraction with 0.15 µl FcR block (anti-mouse CD16/CD32), 0.25 µl anti-mouse CD3-APC and 0.25 µl anti-mouse F4/80-PE antibody (all eBiosciences) for 20 minutes on ice. To assess viability, cells collected during T-cell purification were additionally stained with 0.3 µl propidium iodide (kindly provided by Christian Epp, Heidelberg University Hospital). Cells were measured with a FACS Canto (Becton Dickinson GmbH) and further analyzed using Flowing Software 2.5.1.

SUPPLEMENTARY MATERIAL

Figure S1. Additional examples of immunological pathways that are dysregulated in *Plasmodium*-infected livers (24 h after GAP injection).
Figure S2. Detection and validation of dysregulated miRNAs in infected mice.
Figure S3. Workflow for segregation of hepatocytes and non-parenchymal cells from whole mouse livers using a two-step percoll gradient.
Figure S4. Workflow for further segregation of the non-parenchymal cell fraction from whole mouse livers using a Nycodenz gradient and MACS-based separation and enrichment of Kupffer or T cells.
Figure S5. Further characterization of the workflow from **Supplementary Figure S4**.
Figure S6. Evidence that AAV8 transduces Kupffer cells in murine livers and can be used to purposely dysregulate miR-155.
Table S1. Top networks, genes and regulators affected in GAP-infected mice (Ingenuity analysis).
Table S2. Top networks and genes affected in GAP-infected mice (Metacore analysis).
Table S3. Dysregulated hits in the GAP 24 h group (Ingenuity analysis).
Table S4. Dysregulated hits in the GAP 40-44 h group (Ingenuity analysis).
Table S5. MiRNAs detected in whole liver total RNA with high SNR.
Table S6. Composition of buffers used for cell separation from whole livers.

ACKNOWLEDGMENTS

The authors wish to thank the following people who contributed expertise and help: Jennifer Schahn, Katarina Abramovic, and Miriam Ester (Heidelberg University Hospital, Centre for Infectious Diseases, Parasitology, Heidelberg, Germany) for mosquito breeding and help with malaria infections; Andrea Bauer (German Cancer Research Center, Division of Functional Genome Analysis, Heidelberg, Germany) for support with the cDNA profiling; Justo Lorenzo (Heidelberg University Hospital, Institute of Medical Biometry and Informatics, Heidelberg, Germany) for help with biometrical analyses; Angelika Kretzschmar (Heidelberg University Hospital, Centre for Infectious Diseases, Parasitology, Heidelberg, Germany) for technical assistance with miRNA profiling; Ellen Wiedtke (Heidelberg University Hospital, Centre for Infectious Diseases, Virology, Heidelberg, Germany) for excellent support with AAV vector production and virus purification; Hannah Drescher and Konrad Streetz (Aachen University Hospital, Department of Medicine III, Aachen, Germany) for help with MACS purification of liver cells; as well as Hans-Georg Kräusslich (Heidelberg University Hospital, Centre for Infectious Diseases, Virology, Heidelberg, Germany), Freddy Frischknecht (Heidelberg University Hospital, Centre for Infectious Diseases, Parasitology, Heidelberg, Germany), Adelheid Cerwanka (DKFZ Heidelberg, Germany), and Alexander Dalpke (Heidelberg University Hospital, Centre for Infectious Diseases, Medical Microbiology, Heidelberg, Germany) for reagents, critical discussions, and helpful comments on the manuscript. This study was supported by the University Hospital Heidelberg (to A.-K.M.), the Cluster of Excellence CellNetworks (to D.G., grant number EXC81), the German Center for Infection Research (DZIF) (to K.B.) and the Innovation fond Frontier from the University Heidelberg (to F.H., A.-K.M. and D.G.). F.H., C.H.-K., K.B., K.H., H.W., A.-K.M., and D.G. designed research; F.H., C.H.-K., K.B., K.H., J.M.S., M.C., Y.M., and J.G.B. performed research; B.K. and L.K. analyzed data; and A.-K.M. and D.G. wrote the paper. The authors declare no conflict of interest.

REFERENCES

1. Murray, CJ, Rosenfeld, LC, Lim, SS, Andrews, KG, Foreman, KJ, Haring, D *et al.* (2012). Global malaria mortality between 1980 and 2010: a systematic analysis. *Lancet* **379**: 413–431.
2. Snow, RW, Guerra, CA, Noor, AM, Myint, HY and Hay, SI (2005). The global distribution of clinical episodes of Plasmodium falciparum malaria. *Nature* **434**: 214–217.
3. Lingelbach, K and Joiner, KA (1998). The parasitophorous vacuole membrane surrounding Plasmodium and Toxoplasma: an unusual compartment in infected cells. *J Cell Sci* **111 (Pt 11)**: 1467–1475.
4. Rodrigues, CD, Hannus, M, Prudêncio, M, Martin, C, Gonçalves, LA, Portugal, S *et al.* (2008). Host scavenger receptor SR-BI plays a dual role in the establishment of malaria parasite liver infection. *Cell Host Microbe* **4**: 271–282.
5. Mikolajczak, SA, Jacobs-Lorena, V, MacKellar, DC, Camargo, N and Kappe, SH (2007). L-FABP is a critical host factor for successful malaria liver stage development. *Int J Parasitol* **37**: 483–489.
6. Liehl, P, Zuzarte-Luís, V, Chan, J, Zillinger, T, Baptista, F, Carapau, D *et al.* (2014). Host-cell sensors for Plasmodium activate innate immunity against liver-stage infection. *Nat Med* **20**: 47–53.
7. Nussenzweig, RS, Vanderberg, J, Most, H and Orton, C (1967). Protective immunity produced by the injection of x-irradiated sporozoites of plasmodium berghei. *Nature* **216**: 160–162.

8. Mueller, AK, Labaied, M, Kappe, SH and Matuschewski, K (2005). Genetically modified Plasmodium parasites as a protective experimental malaria vaccine. *Nature* **433**: 164–167.
9. Hoffman, SL, Goh, LM, Luke, TC, Schneider, I, Le, TP, Doolan, DL *et al.* (2002). Protection of humans against malaria by immunization with radiation-attenuated Plasmodium falciparum sporozoites. *J Infect Dis* **185**: 1155–1164.
10. Seder, RA, Chang, LJ, Enama, ME, Zephir, KL, Sarwar, UN, Gordon, IJ *et al.*; VRC 312 Study Team. (2013). Protection against malaria by intravenous immunization with a nonreplicating sporozoite vaccine. *Science* **341**: 1359–1365.
11. Mueller, AK, Deckert, M, Heiss, K, Goetz, K, Matuschewski, K and Schlüter, D (2007). Genetically attenuated Plasmodium berghei liver stages persist and elicit sterile protection primarily via CD8 T cells. *Am J Pathol* **171**: 107–115.
12. Jobe, O, Lumsden, J, Mueller, AK, Williams, J, Silva-Rivera, H, Kappe, SH *et al.* (2007). Genetically attenuated Plasmodium berghei liver stages induce sterile protracted protection that is mediated by major histocompatibility complex Class I-dependent interferon-gamma-producing CD8+ T cells. *J Infect Dis* **196**: 599–607.
13. Trimnell, A, Takagi, A, Gupta, M, Richie, TL, Kappe, SH and Wang, R (2009). Genetically attenuated parasite vaccines induce contact-dependent CD8+ T cell killing of Plasmodium yoelii liver stage-infected hepatocytes. *J Immunol* **183**: 5870–5878.
14. Nganou-Makamdop, K, van Gemert, GJ, Arens, T, Hermsen, CC and Sauerwein, RW (2012). Long term protection after immunization with P. berghei sporozoites correlates with sustained IFN? responses of hepatic CD8+ memory T cells. *PLoS ONE* **7**: e36508.
15. Schofield, L, Villaquiran, J, Ferreira, A, Schellekens, H, Nussenzweig, R and Nussenzweig, V (1987). Gamma interferon, CD8+ T cells and antibodies required for immunity to malaria sporozoites. *Nature* **330**: 664–666.
16. Skalsky, RL and Cullen, BR (2010). Viruses, microRNAs, and host interactions. *Annu Rev Microbiol* **64**: 123–141.
17. Tili, E, Michaille, JJ and Croce, CM (2013). MicroRNAs play a central role in molecular dysfunctions linking inflammation with cancer. *Immunol Rev* **253**: 167–184.
18. Thorn, CF, Lu, ZY and Whitehead, AS (2004). Regulation of the human acute phase serum amyloid A genes by tumour necrosis factor-alpha, interleukin-6 and glucocorticoids in hepatic and epithelial cell lines. *Scand J Immunol* **59**: 152–158.
19. Jopling, C (2012). Liver-specific microRNA-122: Biogenesis and function. *RNA Biol* **9**: 137–142.
20. Chen, CZ, Schaffert, S, Fragoso, R and Loh, C (2013). Regulation of immune responses and tolerance: the microRNA perspective. *Immunol Rev* **253**: 112–128.
21. Tarun, AS, Baer, K, Dumpit, RF, Gray, S, Lejarcegui, N, Frevert, U *et al.* (2006). Quantitative isolation and *in vivo* imaging of malaria parasite liver stages. *Int J Parasitol* **36**: 1283–1293.
22. Pradel, G and Frevert, U (2001). Malaria sporozoites actively enter and pass through rat Kupffer cells prior to hepatocyte invasion. *Hepatology* **33**: 1154–1165.
23. O'Connell, RM, Taganov, KD, Boldin, MP, Cheng, G and Baltimore, D (2007). MicroRNA-155 is induced during the macrophage inflammatory response. *Proc Natl Acad Sci USA* **104**: 1604–1609.
24. Kutty, RK, Nagineni, CN, Samuel, W, Vijayasarathy, C, Hooks, JJ and Redmond, TM (2010). Inflammatory cytokines regulate microRNA-155 expression in human retinal pigment epithelial cells by activating JAK/STAT pathway. *Biochem Biophys Res Commun* **402**: 390–395.
25. O'Connell, RM, Chaudhuri, AA, Rao, DS and Baltimore, D (2009). Inositol phosphatase SHIP1 is a primary target of miR-155. *Proc Natl Acad Sci USA* **106**: 7113–7118.
26. Wang, P, Hou, J, Lin, L, Wang, C, Liu, X, Li, D *et al.* (2010). Inducible microRNA-155 feedback promotes type I IFN signaling in antiviral innate immunity by targeting suppressor of cytokine signaling 1. *J Immunol* **185**: 6226–6233.
27. van Dijk, R, Montenegro-Miranda, PS, Riviere, C, Schilderink, R, ten Bloemendaal, L, van Gorp, J *et al.* (2013). Polyinosinic acid blocks adeno-associated virus macrophage endocytosis *in vitro* and enhances adeno-associated virus liver-directed gene therapy in vivo. *Hum Gene Ther* **24**: 807–813.
28. Grimm, D, Streetz, KL, Jopling, CL, Storm, TA, Pandey, K, Davis, CR *et al.* (2006). Fatality in mice due to oversaturation of cellular microRNA/short hairpin RNA pathways. *Nature* **441**: 537–541.
29. Faraoni, I, Antonetti, FR, Cardone, J and Bonmassar, E (2009). miR-155 gene: a typical multifunctional microRNA. *Biochim Biophys Acta* **1792**: 497–505.
30. Monk, CE, Hutvagner, G and Arthur, JS (2010). Regulation of miRNA transcription in macrophages in response to Candida albicans. *PLoS ONE* **5**: e13669.
31. Bala, S, Tilahun, Y, Taha, O, Alao, H, Kodys, K, Catalano, D *et al.* (2012). Increased microRNA-155 expression in the serum and peripheral monocytes in chronic HCV infection. *J Transl Med* **10**: 151.
32. Ghorpade, DS, Leyland, R, Kurowska-Stolarska, M, Patil, SA and Balaji, KN (2012). MicroRNA-155 is required for Mycobacterium bovis BCG-mediated apoptosis of macrophages. *Mol Cell Biol* **32**: 2239–2253.
33. Cai, P, Piao, X, Liu, S, Hou, N, Wang, H and Chen, Q (2013). MicroRNA-gene expression network in murine liver during Schistosoma japonicum infection. *PLoS ONE* **8**: e67037.
34. Cremer, TJ, Ravneberg, DH, Clay, CD, Piper-Hunter, MG, Marsh, CB, Elton, TS *et al.* (2009). MiR-155 induction by F. novicida but not the virulent F. tularensis results in SHIP down-regulation and enhanced pro-inflammatory cytokine response. *PLoS ONE* **4**: e8508.
35. Rodriguez, A, Vigorito, E, Clare, S, Warren, MV, Couttet, P, Soond, DR *et al.* (2007). Requirement of bic/microRNA-155 for normal immune function. *Science* **316**: 608–611.
36. Oertli, M, Engler, DB, Kohler, E, Koch, M, Meyer, TF and Müller, A (2011). MicroRNA-155 is essential for the T cell-mediated control of Helicobacter pylori infection and for the induction of chronic Gastritis and Colitis. *J Immunol* **187**: 3578–3586.
37. Vigorito, E, Perks, KL, Abreu-Goodger, C, Bunting, S, Xiang, Z, Kohlhaas, S *et al.* (2007). microRNA-155 regulates the generation of immunoglobulin class-switched plasma cells. *Immunity* **27**: 847–859.
38. Thai, TH, Calado, DP, Casola, S, Ansel, KM, Xiao, C, Xue, Y *et al.* (2007). Regulation of the germinal center response by microRNA-155. *Science* **316**: 604–608.
39. O'Connell, RM, Kahn, D, Gibson, WS, Round, JL, Scholz, RL, Chaudhuri, AA *et al.* (2010). MicroRNA-155 promotes autoimmune inflammation by enhancing inflammatory T cell development. *Immunity* **33**: 607–619.
40. Gracias, DT, Stelekati, E, Hope, JL, Boesteanu, AC, Doering, TA, Norton, J *et al.* (2013). The microRNA miR-155 controls CD8(+) T cell responses by regulating interferon signaling. *Nat Immunol* **14**: 593–602.
41. Zhang, Y, Wei, W, Cheng, N, Wang, K, Li, B, Jiang, X *et al.* (2012). Hepatitis C virus-induced up-regulation of microRNA-155 promotes hepatocarcinogenesis by activating Wnt signaling. *Hepatology* **56**: 1631–1640.
42. Chang, S, Wang, RH, Akagi, K, Kim, KA, Martin, BK, Cavallone, L *et al.*; Kathleen Cuningham Foundation Consortium for Research into Familial Breast Cancer (kConFab). (2011). Tumor suppressor BRCA1 epigenetically controls oncogenic microRNA-155. *Nat Med* **17**: 1275–1282.
43. O'Connell, RM, Rao, DS, Chaudhuri, AA, Boldin, MP, Taganov, KD, Nicoll, J *et al.* (2008). Sustained expression of microRNA-155 in hematopoietic stem cells causes a myeloproliferative disorder. *J Exp Med* **205**: 585–594.
44. Kurowska-Stolarska, M, Alivernini, S, Ballantine, LE, Asquith, DL, Millar, NL, Gilchrist, DS *et al.* (2011). MicroRNA-155 as a proinflammatory regulator in clinical and experimental arthritis. *Proc Natl Acad Sci USA* **108**: 11193–11198.
45. Worm, J, Stenvang, J, Petri, A, Frederiksen, KS, Obad, S, Elmén, J *et al.* (2009). Silencing of microRNA-155 in mice during acute inflammatory response leads to derepression of c/ebp Beta and down-regulation of G-CSF. *Nucleic Acids Res* **37**: 5784–5792.
46. Huffaker, TB, Hu, R, Runtsch, MC, Bake, E, Chen, X, Zhao, J *et al.* (2012). Epistasis between microRNAs 155 and 146a during T cell-mediated antitumor immunity. *Cell Rep* **2**: 1697–1709.
47. Clare, S, John, V, Walker, AW, Hill, JL, Abreu-Goodger, C, Hale, C *et al.* (2013). Enhanced susceptibility to Citrobacter rodentium infection in microRNA-155-deficient mice. *Infect Immun* **81**: 723–732.
48. Miller, AM, Gilchrist, DS, Nijjar, J, Araldi, E, Ramirez, CM, Lavery, CA *et al.* (2013). MiR-155 has a protective role in the development of non-alcoholic hepatosteatosis in mice. *PLoS ONE* **8**: e72324.
49. Aucher, A, Rudnicka, D and Davis, DM (2013). MicroRNAs transfer from human macrophages to hepato-carcinoma cells and inhibit proliferation. *J Immunol* **191**: 6250–6260.
50. Kota, J, Chivukula, RR, O'Donnell, KA, Wentzel, EA, Montgomery, CL, Hwang, HW *et al.* (2009). Therapeutic microRNA delivery suppresses tumorigenesis in a murine liver cancer model. *Cell* **137**: 1005–1017.
51. Janssen, HL, Reesink, HW, Lawitz, EJ, Zeuzem, S, Rodriguez-Torres, M, Patel, K *et al.* (2013). Treatment of HCV infection by targeting microRNA. *N Engl J Med* **368**: 1685–1694.
52. Ebert, MS, Neilson, JR and Sharp, PA (2007). MicroRNA sponges: competitive inhibitors of small RNAs in mammalian cells. *Nat Methods* **4**: 721–726.
53. Heymans, S, Corsten, MF, Verhesen, W, Carai, P, van Leeuwen, RE, Custers, K *et al.* (2013). Macrophage microRNA-155 promotes cardiac hypertrophy and failure. *Circulation* **128**: 1420–1432.
54. Schürmann, N, Trabuco, LG, Bender, C, Russell, RB and Grimm, D (2013). Molecular dissection of human Argonaute proteins by DNA shuffling. *Nat Struct Mol Biol* **20**: 818–826.
55. Börner, K, Niopek, D, Cotugno, G, Kaldenbach, M, Pankert, T, Willemsen, J *et al.* (2013). Robust RNAi enhancement via human Argonaute-2 overexpression from plasmids, viral vectors and cell lines. *Nucleic Acids Res* **41**: e199.
56. Castoldi, M, Vujic Spasic, M, Altamura, S, Elmén, J, Lindow, M, Kiss, J *et al.* (2011). The liver-specific microRNA miR-122 controls systemic iron homeostasis in mice. *J Clin Invest* **121**: 1386–1396.
57. Hellemans, J, Mortier, G, De Paepe, A, Speleman, F and Vandesompele, J (2007). qBase relative quantification framework and software for management and automated analysis of real-time quantitative PCR data. *Genome Biol* **8**: R19.
58. Froh, M, Konno, A and Thurman, RG (2003). Isolation of liver Kupffer cells. *Curr Protoc Toxicol* **Chapter 14**: Unit14.4.